Sound & Vibration 2026, 60(5), 4463.
doi: https://doi.org/10.59400/sv4463

Article

Thermoacoustic loss-of-chaos in large diesel engines: Case study on long-timescale events

Alice Elizabeth González[1,*], Pablo Gianoli-Kovar[1], Héctor Campello-Vicente[2]

[1] Environmental Engineering Department, Faculty of Engineering, Universidad de la República, Montevideo 11200, Uruguay
[2] Engineering Research Institute of Elche I3E, Universidad Miguel Hernández de Elche, 03202 Elche, Spain
*** Corresponding author:** Alice Elizabeth González, elizabet@fing.edu.uy

CITATION

González AE, Gianoli-Kovar P, Campello-Vicente H. Thermoacoustic loss-of-chaos in large diesel engines: Case study on long-timescale events. Sound & Vibration. 2026; 60(5): 4463.
https://doi.org/10.59400/sv4463

ARTICLE INFO

Received: 29 May 2026
Revised: 28 June 2026
Accepted: 9 July 2026
Available online: 27 July 2026

Abstract: This work aims to analyze the occurrence of anomalous acoustic emissions that appeared after the modification of the combustion chambers of eight reconverted four-stroke diesel engines (10 MW each, urban installation). Large variability of the sound pressure levels emitted by the same engine under nominally identical operating conditions was recorded. The phenomenon was interpreted at first as thermoacoustic instability developing inside the combustion chambers, supported by the simultaneous observation of large fluctuations in the fuel inlet pressure. Four precursor episodes were documented through an operational signature qualitatively consistent with the loss-of-chaos pattern reported in the literature. However, most of these events anticipated a decrease in the sound pressure levels in the considered third-octave band, the opposite of what is expected to happen in thermoacoustic instability events. The 0–1 test for loss-of-chaos was applied, ratifying the occurrence of a long precursor condition that should anticipate the installation of a thermoacoustic instability. The shortest timescale of the precursor states was 500 s, in contrast with the millisecond- to second-range timescales typically reported in laboratory-scale studies. Although the sample is limited, the observations suggest that long precursors may occur in megawatt-scale installations, anticipating different types of sudden changes in the operational conditions (not only thermoacoustic instability). If confirmed, it would open a practical window for feedforward active noise control to avoid abrupt changes in the engine operating conditions. A hybrid silencing strategy is proposed as a design recommendation. Limitations and the current operational status of the installation are also discussed.

Keywords: large diesel engines; combustion noise; loss of chaos; active noise control

1. Introduction

Internal combustion engines operating as electrical generators are among the most relevant industrial noise sources because of the high sound power levels associated with their operating principle [1, 2]. Two main acoustic emission mechanisms are usually distinguished: combustion roar, associated with stable operation [1], which is "a band-limited pseudo-random sound" [3]; and noise produced by thermoacoustic instabilities, linked to fluid oscillations developing during combustion, also called "combustion-driven oscillation, combustion dynamic instability, and thermoacoustic instability" [3]. This acoustic oscillation causes large pressure fluctuations, which manifest as high sound pressure levels. It can also cause combustion inefficiency, increased emissions, and structural damage to combustion chambers.

Combustion noise is the dominant source in diesel engines [4, 5]. It depends on engine speed, load, injection strategy, fuel composition and ignition delay. Although a strong correlation between in-cylinder pressure and emitted noise has been reported [4], the noise is largely caused by the stochastic nature of combustion, with broadband random fluctuations dominating the in-cylinder pressure [4,5]. Combustion fluctuations may be amplified when engine operation is optimized—for example, to minimize fuel consumption or to achieve a target exhaust composition—since combustion dynamics is a non-linear, multidimensional process mediated by stochastic fluctuations [5].

Thermoacoustic instabilities arise from the phase-amplitude coupling between pressure oscillations and unsteady heat release. The Rayleigh Index, defined as the spatiotemporally integrated product of pressure and heat-release fluctuations, quantifies this coupling: positive values indicate net amplification. Experimental work on premixed burners has shown that this index remains positive under steady operating conditions even with out-of-phase responses, owing to the non-linear character of the flame response [6]. Pressure oscillations may also modulate the injector mass-flow rate, producing positive feedback; simulations of full annular combustors have shown that a large fraction of the acoustic energy concentrates in low-order transverse modes requiring active suppression [7]. Adaptive feedback control systems based on piezoresistive microphones and membrane actuators achieve substantial reductions of exhaust noise through destructive interference of low-frequency waves [8,9].

Three frequency regimes can be distinguished in the unsteady combustion response [5]:

- Low-frequency oscillations (approximately 4–70 Hz) are associated with non-homogeneous propagation of the flame front and have long characteristic time constants, which links them to low-frequency emissions.
- In the 70–700 Hz range, stationary waves with different phase angles develop, with characteristic time constants of the order of 3–6 ms.
- Phenomena at high frequencies show characteristic time constants of approximately 0.5 ms.

The rotational frequencies of large electric generators fall within the range associated with flame-front fluctuations, so a coupling between this phenomenon and the operating frequencies of the equipment could result in significant acoustic emissions.

1.1. Advances in thermoacoustic instability research

Poinsot [10] reviewed the advances in the prediction and control of thermoacoustic instabilities in propulsion engines, identifying the fundamental differences between laboratory burners and real engines. In full-scale systems, new mechanisms emerge owing to higher Reynolds numbers, greater power densities, multiple inlet systems and complex fuel compositions, as well as direct coupling between the chamber acoustics and the surrounding turbomachinery—a situation directly relevant to the engines studied here. Juniper and Sujith [11] reviewed the sensitivity and nonlinear character of thermoacoustic oscillations, explaining how non-periodic and chaotic behaviour arise from the underlying nonlinear dynamics, and providing a theoretical basis for understanding the variability of acoustic emissions observed in the present case. Sujith and Unni [12] developed a complex-systems perspective, framing the transition from stochastic combustion noise to thermoacoustic instability as an emergent behaviour, and showing how tools from network theory and synchronization can support both early diagnosis and mitigation.

From the perspective of diesel engine acoustics, Broatch et al. [13] showed via large eddy simulations (LES) that the acoustic signature of a compression-ignition engine is governed by the intensity of the premixed combustion phase rather than by turbulent fluctuations in the diffusion stage—a finding directly relevant to the present study, where modifications to the combustion chambers altered the premixed combustion characteristics. From a control perspective, Magri [14] demonstrated that adjoint-based sensitivity analysis efficiently identifies the parameters and spatial locations to which thermoacoustic stability is most sensitive, enabling the rational design of passive and active control strategies. Together, these contributions show that thermoacoustic instabilities in real engines constitute a multi-scale, highly sensitive problem for which no single diagnostic or control approach is universally effective.

Regarding thermoacoustic instability control techniques, Deshmukh et al. [15,16] note that they can be classified as passive or active, with passive techniques being the least flexible and adaptable. Active control techniques are more frequently used not only because of their greater adaptability and flexibility but also because of their lower cost. These techniques include not only generating an inverse sound wave to counteract the instability's effect but also methods for controlling its generation through air or fuel injection. The authors developed radial air injection systems, both open-loop and closed-loop, to control thermoacoustic instabilities, which proved effective at the laboratory scale. Zhu et al. and George et al. [17,18] note that passive control methods aim to modify the acoustic energy balance to prevent an increase in disturbance. Just the opposite to Deshmukh et al. [15, 16], they affirm that passive control is more reliable and does not require predictions for its activation. They also believe that passive control is easier to implement. The authors mention the use of acoustic dampers (such as Helmholtz resonators and perforated plates) to increase acoustic energy dissipation, keep the equivalence ratio away from the instability limit, or directly adjust the burner structure. They present a passive control device for a domestic gas stove that works by fine-tuning the burner nozzle structure. By adding perforated plates, they manage to suppress the thermoacoustic instability that occurs at mid-frequencies. Deng et al. [19] propose controlling thermoacoustic instabilities by plasma discharges; they work at laboratory scale using a Rijke tube and they succeeded in suppressing the instabilities. Gosavi and Priyam [20] mention several successful experiences in vibration and noise control using active methods related to internal combustion engines of vehicles, but they do not analyze their application on another scale of combustion engines.

When studying large reciprocating machines, strong simplifications must be avoided: in particular, the assumption of instantaneous and homogeneous combustion within each cylinder, acceptable for laboratory-scale combustors, becomes invalid in the megawatt regime considered here.

1.2. Relation to previous work and contribution of the present study

A preliminary description of the same installation, including the experimental layout and the first attribution of the acoustic anomaly to thermoacoustic phenomena, was provided by González et al. [21]. The present work re-examines and extends that material in three respects: (i) it integrates the case into the broader framework of complex-systems approaches to combustion instability [11, 12]; (ii) it documents in detail the temporal evolution of the loss-of-chaos signature in selected one-third octave bands (TOB) during four representative episodes, and provides a comparative reading of these durations against the laboratory-scale literature, specially by applying an exploratory analysis based on the 0–1 test for loss of chaos [22, 23]; and (iii) it formulates a noise-control design recommendation explicitly based on the observed precursor timescale. The experimental data underpinning the present analysis are largely those collected during the campaign reported in the work of González et al. [21]; this is made explicit throughout the manuscript.

2. Materials and methods

2.1. Description of the installation

The case study refers to a set of eight 10 MW reconverted four-stroke diesel engines with 12 cylinders installed in an urban area and generating alternating current at 50 Hz. They are very large units: each engine has a length of 12.6 m and has a cross-section of approximately 3.6 m × 5.1 m. Each generator has six pairs of poles; the engines therefore rotate at 500 rpm (8.33 Hz). Two years after commissioning, modifications were introduced to comply with NO_x emission specifications: the combustion chambers were redesigned and a turbocharger group operating at 25,500 rpm (425 Hz) was installed in each engine. While the NO_x specification was successfully met, anomalous acoustic emissions subsequently appeared—in particular, a marked variability of the sound pressure levels emitted by the same engine under nominally identical operating conditions, with only a few hours between successive measurements [21]. The research team was originally engaged to identify the causes of these acoustic phenomena and to propose noise-control measures; the study was not initially designed to investigate thermoacoustic instabilities, which were eventually identified as the possible underlying mechanism. Another outcome of the analysis was that the development time of the precursor signals before the change of operation condition of the engine: it was of the order of several minutes—in contrast to the millisecond- to second-range timescales reported in the laboratory-scale literature—and this is the central observation around which the present work is organized.

The engines are four-stroke diesel units in which fuel ignition is initiated by the high compression generated within the chamber. The idealized cycle delivers one useful power stroke every two crankshaft revolutions, so each cylinder fires every two revolutions. The engine speed is 500 rpm (8.33 Hz) and is maintained by automatic regulation within ±1% of the nominal value. With twelve cylinders firing on alternate revolutions at 8.33 Hz, six cylinders fire per revolution, yielding a fundamental firing rate of 50 Hz that coincides with the grid frequency; this coincidence will become relevant in Section 4. The fuel mass per cycle is modulated according to operating conditions, controlling the maximum compression pressure. Air is drawn from outside through ducts crossing the chamber walls and is filtered before being admitted to the engine. Each engine is equipped with an individual passive silencer at its outlet and an individual 60 m exhaust stack [21].

The engines are installed in a 51 m × 37 m × 19 m (approximately) room. They are arranged in two parallel lines of four units, with symmetrical exhaust ducts leading to the stacks. The shortest duct is more than 17 m long, while the shortest fuel line is more than 12 m. The stacks (approximately 1.5 m in diameter) are constructed from steel sheet metal. Two of the eight engines are additionally fitted with a heat recovery boiler in their exhaust line, used to generate steam for auxiliary services such as fuel-viscosity reduction [21].

The noise emitted by reciprocating engines is largely produced by the stochastic nature of combustion. Depending on the difference between convection and acoustic times, entropy waves may couple constructively or destructively with the chamber acoustics, and a qualitative analysis is generally insufficient to determine whether this coupling is strong enough to significantly affect thermoacoustic stability. In general, combustion instability can be understood as a resonant interaction between at least two oscillatory mechanisms—an excitation mechanism and a feedback effect—whose relative phase determines whether the interaction enhances or suppresses the susceptibility to thermoacoustic oscillations. In the case reported here, no instabilities were observed in the heat release rate, as inferred from the stable electrical power output; nevertheless, abrupt changes in the sound pressure levels emissions—that showed changes in the engine operating conditions—occurred, as it could be verified when applying objective detection methods (see Section 3).

Following Schuermans [24], fluctuations in fuel concentration are a major (though not the only) cause of the interaction between heat release and the acoustic field. The underlying issue is that the idealized processes assumed in small-scale combustion—instantaneous ignition, homogeneous mixture, instantaneous and complete combustion within each cylinder—become invalid at the megawatt scale. Thermoacoustic oscillations also cause accelerated wear of engine components, impose mechanical loads on chamber walls, increase heat transfer to the liner through non-stationary flow, and may compromise the electronic systems controlling combustion. Large thermoacoustic oscillations are therefore undesirable in every combustion chamber.

2.2. Experimental campaign

An experimental campaign of controlled operation tests was designed and executed. It is worth saying that this measurement campaign aimed to obtain a diagnosis of what was happening with acoustic emissions and not to study in depth the phenomena of thermoacoustic large oscillations or even instability, since they had not been identified at that time. The tests consisted of a predefined sequence of switching the engines on and off one by one, with simultaneous recordings of sound pressure levels in one-third octave bands at three measurement points. Sound pressure levels were recorded as TOB Z-weighted equivalent levels (L_{Zeq}), preserving the low-frequency content without frequency-weighting filters; this is the natural choice for diagnosis of low-frequency combustion phenomena. Three Class 1 sound level meters (IEC 61672) were used: two Brüel & Kjær Model 2250 and one Cirrus device, with valid calibration certificates throughout the campaign. The bands processed in the present analysis span from 6.3 Hz to 3.15 kHz, with particular attention to those at 8, 12.5, 25, 40, 50, 63 and 125 Hz, where the relevant phenomena were observed. The on/off sequence proceeded as follows: one engine was started and operated alone for 30 min; a second engine was then started and both engines operated jointly for 30 min; the first engine was subsequently switched off and the second operated alone for 30 min; and so on, until each engine had been recorded operating in isolation for 30 min [21].

Processing of the measurements yielded several unexpected results. In some TOB and at the measurement point closest to the engines (**Figures 1–3**), all of the following situations were registered when an individual engine was switched on or off:

- The sound pressure level remained unchanged;
- The sound pressure level decreased by 3 dB, as would be expected on energetic grounds;
- The sound pressure level decreased by more than 3 dB;
- The sound pressure level increased by 3 dB;
- The sound pressure level increased by more than 3 dB.

All these figures were elaborated by the authors from the experimental data.

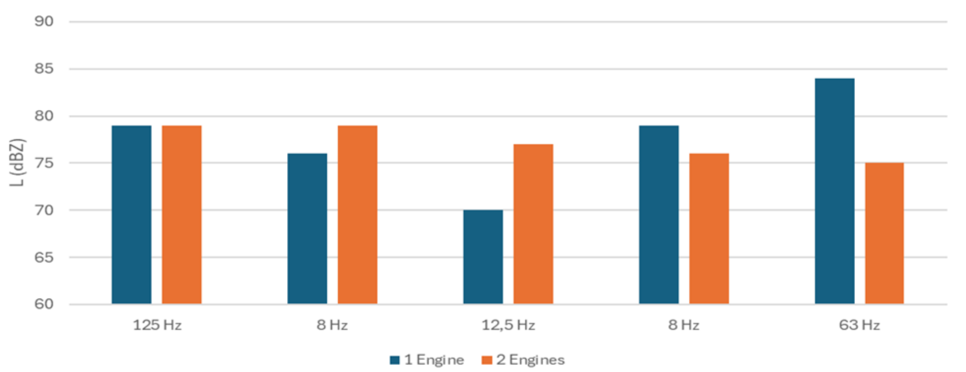

Figure 1. Examples of non-monotonic variations of Z-weighted sound pressure levels in selected TOB when switching individual engines on or off.

Note: Measurement point closest to the engines; Class 1 sound level meter (IEC 61672). Comparison between operation with one and two engines for nominally identical operating conditions.

The sound pressure levels emitted by the same engine differed substantially between successive tests, both in their global levels and in their spectral distribution. Particularly informative were the differences in the emission spectra of the same engine under identical operating conditions across two 30-min episodes: discrepancies of up to 10 dB were observed in individual TOB, with the sign of the discrepancy inconsistent between bands and between episodes. When the measured sound pressure levels were compared with those predicted by conventional acoustic modelling, the largest deviations appeared in the bands centered at 25 Hz, 63 Hz and 125 Hz. Records taken inside the engine room confirmed that, for the same operating configuration and electrical power output, some bands exhibited substantial fluctuations that were not apparent in the broadband levels [21].

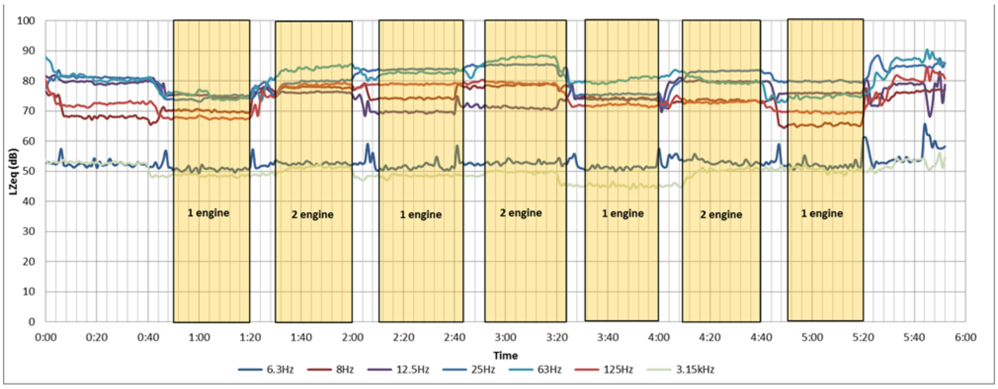

Figure 2. Time evolution of Z-weighted equivalent sound pressure levels (L_{Zeq}) in selected TOB (6.3, 8, 12.5, 25, 63, 125 Hz and 3.15 kHz) under an alternating one-engine/two-engine operating sequence over approximately six hours.

Note: The non-monotonic response of several low-frequency bands when an engine is switched off.

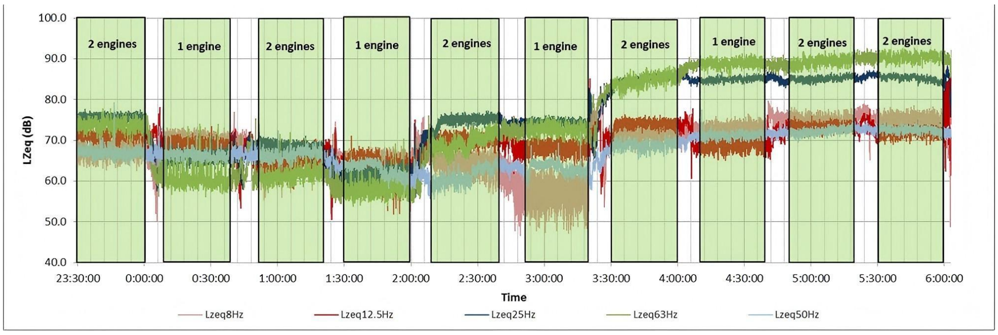

Figure 3. Time evolution of Z-weighted equivalent sound pressure levels (L_{Zeq}) in selected TOB (8, 12.5, 25, 50 and 63 Hz) under a different alternating sequence.

Note: The marked jump in the 25 Hz band shortly after 03:30 illustrates the abrupt nature of the level transitions associated with the phenomenon.

In the second stage of the experimental campaign, the sound power level of each engine was determined following ISO 3744:2010 [25]. A Class 1 (IEC 61672) Brüel & Kjær Model 2250 sound level meter was used, together with its tripod and an extension pole for elevated measurements. The environmental sound pressure levels inside the engine room were recorded simultaneously.

During the first ISO 3744 campaign, large fluctuations were observed in the fuel inlet pressure of the engines. This information was not publicly accessible from the engine control system, but the magnitude of the fluctuations in the fuel supply line was an unambiguous indication of the development of combustion instabilities. As is well established in the literature, any modification of the combustion conditions modifies the associated acoustic emissions; therefore, the appearance of these phenomena following the redesign of the combustion chambers should have been foreseeable. Two coupled problems were thereby identified: how to predict the occurrence of large thermoacoustic oscillations and instabilities, and how to control the noise emission associated with them.

2.3. The 0–1 test for chaos as a diagnostic reference

The reference framework for diagnosing impending thermoacoustic instability is the 0–1 test for chaos, originally proposed by Gottwald and Melbourne [22, 23] and applied to combustion noise by Nair et al. [26]. The 0–1 test provides an objective, binary-valued indicator of the chaotic or regular nature of a time series without requiring phase-space reconstruction or knowledge of the underlying dynamical model. Its main advantages, particularly in industrial settings, are its computational efficiency and its independence from combustor geometry, fuel type or other system-specific features.

Given a scalar time series φ(j), j = 1, …, N (in the present context, either an in-cylinder pressure signal or a sound pressure signal), and a chosen frequency $c \in (0, \pi)$, the test constructs the two translation variables:

$$\mathrm{p(n)} = \sum\nolimits_{\mathrm{j}\,=\,1}^{\mathrm{n}} \varnothing(\mathrm{j})\cos(\mathrm{jc})$$

$$\mathrm{q(n)} = \sum\nolimits_{\mathrm{j}\,=\,1}^{\mathrm{n}} \varnothing(\mathrm{j})\sin(\mathrm{jc})$$

with $n = 1, \ldots, N$, and the time-averaged mean square displacement of the resulting trajectory in the (p, q) plane. The asymptotic growth rate K of this mean square displacement is then computed; K tends to 0 for regular (non-chaotic) dynamics and to 1 for chaotic dynamics. In the context of combustion noise, the transition from a chaotic state (broadband stochastic combustion) to a regular state (coherent thermoacoustic oscillation) is reflected by a decrease of K from values close to 1 towards values close to 0, and this decrease can be used as an early-warning indicator of impending instability [26].

In the present work, a full numerical application of the 0–1 test to the recorded time series was undertaken, obtaining the sound pressure from the high-rate raw recorded sound pressure levels (one data per second in every TOB and in broad band). No other raw data was available from the original campaigns. The loss of chaos was instead identified through the temporal evolution of the L_{Zeq} levels in selected TOB—primarily 25 Hz and 50 Hz—where the precursor signature was clearest. The visual signature considered to indicate loss of chaos is the transition of the band-level trace from a regime of dense, fast variability (a broad envelope around the local mean) to a regime of smoother evolution with reduced short-time variance, preceding the sudden jump in sound pressure levels associated with the onset of the instability. This is therefore only a qualitative inference of the loss-of-chaos pattern described by Nair et al. [26].

To complement the temporal analysis of the frequencies of interest and reduce the subjectivity associated with the visual inspection of precursor signals, an exploratory analysis was performed based on the principles of the 0–1 test for chaos proposed by Gottwald and Melbourne [22,23]. While there are free codes for the implementation of the test [27], we developed an exploratory version of it. This implementation did not apply the complete procedure of the original method but rather a simplified adaptation aimed at evaluating the dynamic evolution of different representative time windows using quantitative indicators.

As a starting point, the sound pressure levels recorded for each frequency band,

$L_p(j)$, were converted to instantaneous acoustic pressure using:

$$p(j) = p_0 10^{L_p(j)/20}$$

where:

- $p(j)$ is the sound pressure at time j,
- $L_p(j)$ is the sound pressure level at the considered TOB,
- $p_0 = 20$ μPa is the reference sound pressure.

Subsequently, to eliminate the average value of each window and analyze only the temporal fluctuations, the centered signal was constructed:

$$\varnothing(j) = p(j) - \bar{p}$$

where

- $\phi(j)$ is the centered signal,
- $\bar{p}$ is the mean value of the root-mean-square values of sound pressure in the considered window.

The signal $\phi(j)$ constitutes the input variable used in the exploratory analysis. Following the formulation proposed by Gottwald and Melbourne [22, 23], the translation variables were constructed:

$$p(n) = \sum_{j=1}^{n} \varnothing(j)\cos(jc)$$

$$q(n) = \sum_{j=1}^{n} \varnothing(j)\sin(jc)$$

The variables $p(n)$ and $q(n)$ represent the coordinates of a two-dimensional trajectory obtained by integrating the signal modulated by trigonometric functions. Conceptually, this transformation allows to represent the time evolution of the signal in a new dynamic space, where confined trajectories are usually associated with a more regular behaviour, while expansive ones indicate more complex dynamics. In these expressions, c takes values between 0 and π. To minimize possible numeric resonances associated with certain values of c, Gottwald and Melbourne recommend selecting values within the approximate range:

$$\frac{\pi}{5} < c < \frac{4\pi}{5}$$

We varied c values from 0.6 to 2.5 (recommended range [23]) with a step of 0.01, and selected the c value that maximizes the value of the test parameter K [23].

The mean square displacement M(n) was calculated from the previous trajectories [23]:

$$M(n) = \frac{1}{N-n} \sum_{j=1}^{N-n} \left[(p(j+n) - p(j))^2 + (q(j+n) - 1(j))^2 \right]$$

where:

- N corresponds to the total amount of data in the analysed window.
- n represents the considered time delay.

From a conceptual standpoint, $M(n)$ quantifies the average displacement experienced by the trajectory $(p,\ q)$ when comparing points separated by a delay n. Small values of $M(n)$ indicate relatively confined trajectories, while a progressive increase in $M(n)$ reflects a greater expansion of the reconstructed dynamics.

While the most common applications of the test are in laboratory-scale installations, its foundations lie in dynamical systems theory; therefore, it is applicable to various time series to determine whether they follow regular or chaotic dynamics. Hence, the test is applicable to both full-scale and laboratory installations, regardless of the scale of the case.

In the present study, time windows of 1,000 data points, equivalent to 1,000 s (16.67 min) of recording, were analyzed. They were selected according to the different regimes observed in the time evolution of each frequency of interest. For each window, the root mean square displacement was calculated for only seven representative delays: $n = \{1, 10, 25, 50, 100, 200, 300\}$.

This selection allowed for the coverage of short, medium, and long timescales within each window, while maintaining a sufficient number of pairs available to calculate $M(n)$. The use of this reduced set of delays was based on criteria of computing efficiency and simplicity of implementation, since the objective of the analysis was not to exhaustively reproduce the original algorithm, but rather to characterize the growth trend of the mean shift in each time regime.

Assuming a potential relationship between $M(n)$ and n, the relationship was plotted on a logarithmic scale, and a straight line was fitted using least-squares linear regression:

$$\ln[M(n)] = a + K_{exp}\ln(n)$$

where K_{exp} corresponds to the adjusted slope.

It is important to note that this parameter does not correspond to the K value defined in the formal implementation of the 0–1 test, but rather constitutes an exploratory indicator of the growth of $M(n)$. Steep slopes indicate a faster expansion of the reconstructed trajectory, while gentle slopes reflect more confined trajectories (that's why we attempted to maximize the value of K_{exp} for selecting the value of c, i.e., the highest value of K_{exp} corresponds to the most chaotic operational condition occurred in the considered window).

As a complementary indicator, the value of $M(300)$ was considered; it corresponds to the root mean square shift for the largest analyzed delay (5 min or 300 s). This parameter allowed for comparison of the absolute expansion of the reconstructed trajectories in the different time windows.

Finally, for each window, the following parameters were analyzed together:

- The time evolution of the centred signal $\phi(j)$;
- The exploratory slope K_{exp};
- The mean square displacement $M(n)$;
- The representation of the trajectory in the plane $(p,\ q)$;

- The numerical value of M(300);
- The standard deviation of the centred signal.

The combined interpretation of these indicators allowed for an objective characterization of the dynamic evolution of the different time windows, identifying relatively confined regimes and regimes with greater expansion of the reconstructed trajectories. In this way, the exploratory analysis provided a quantitative tool complementary to the visual inspection of precursor signals, reducing subjectivity in the identification of dynamic changes prior to instability events.

3. Results

3.1. Variability of sound pressure levels across the spectrum

The acoustic measurements obtained during the on/off operation tests (Section 2.2) revealed that the sound pressure level changes associated with switching of individual engines did not follow the energetic expectation of a −3 dB decrease per engine turned off (**Figures 1–3**). Five distinct types of response were observed across the TOB spectrum, as listed in Section 2.2. The departures from the expected behavior were particularly pronounced in the bands centered at 25, 63 and 125 Hz, where differences of up to 10 dB were recorded between two 30-min episodes of the same engine operating under identical nominal conditions. These observations cannot be explained by the conventional combustion-roar mechanism alone and pointed to a dynamic phenomenon affecting the acoustic source itself.

3.2. Fuel inlet pressure as an indicator of combustion instability

During the determination of individual sound power levels according to ISO 3744:2010 [25], large fluctuations of the fuel inlet pressure were observed (**Figure 4**). The magnitude of these fluctuations was inconsistent with stable combustion and constituted an unambiguous indication of the development of large pressure oscillations within the combustion chambers. This finding linked the spectral variability described in Section 3.1 to a physical mechanism originating inside the engines themselves.

(a) (b)

Figure 4. Engine control commands during testing according to ISO 3744:2010: **(a)** Fuel pressure at its near-maximum point (16 bar); **(b)** Fuel pressure at zero, 6 s later.

3.3. Loss-of-chaos signature as a precursor of a change in the operation condition

The sound pressure levels in the engine room were recorded in TOB during the ISO 3744 tests of the 8 engines, using a fixed Class 1 sound level meter. While analyzing the registers, during two of the 8 tests, we observed the occurrence of a characteristic pattern in the 25 Hz and 50 Hz TOB, qualitatively consistent with the loss-of-chaos signature described by Nair et al. [26] (see Section 2.3). In total, we registered four episodes, which are reported in **Figures 5–8**; in two of them, the pattern appeared simultaneously in the 25 Hz and 50 Hz BTO. All these figures were elaborated by the authors from the experimental data. In all cases, the loss-of-chaos pattern was observed to persist for several minutes before a sudden change in the operation condition of the engine.

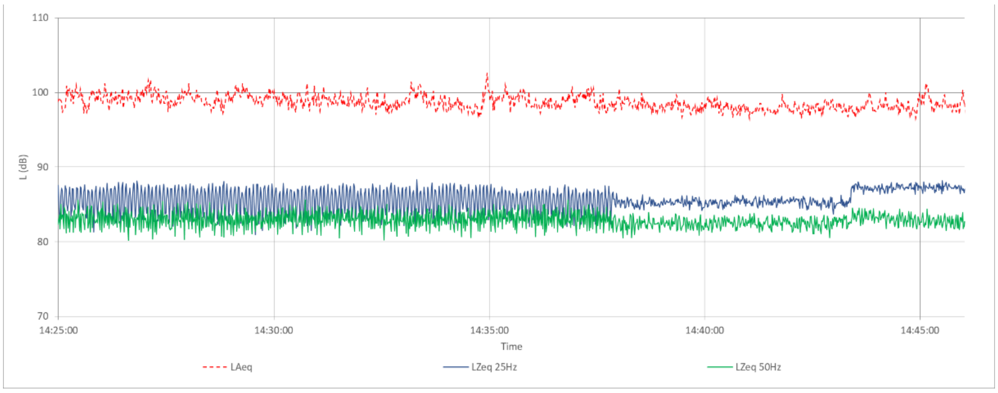

Figure 5. Loss-of-chaos signature in the 25 Hz TOB during the development of a thermoacoustic instability episode (single engine in operation, ISO 3744 [25] testing).
Note: The trace at 25 Hz (blue) shows a transition from a non-chaotic situation to a smoother regime; the 50 Hz band (green) is shown for comparison.

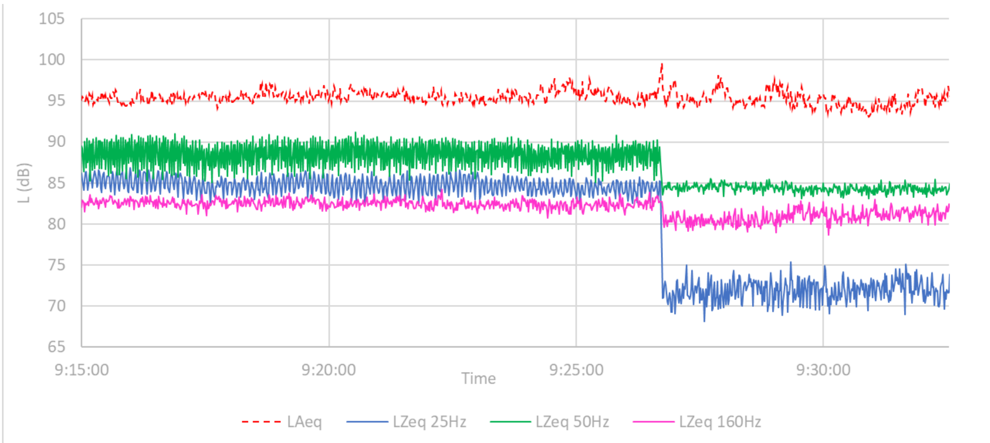

Figure 6. Loss-of-chaos signature simultaneously affecting the 25 Hz and 50 Hz bands during ISO 3744 [25] testing (single engine in operation).
Note: Sudden negative changes are observed: a decrease of 10 dB at 25 Hz (blue) and approximately 5 dB at 50 Hz (green) and 3 dB at 160 Hz.

3.4. Outcomes of the exploratory analysis based on the 0–1 test for chaos

A summary of the main characteristics of the precursor episodes documented in **Figures 5–8** and the outcomes of the exploratory analysis is provided in **Tables 1** and **2**.

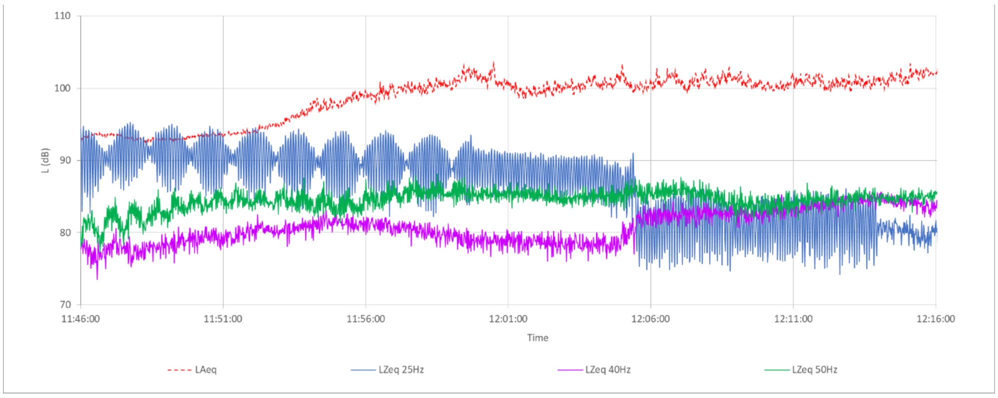

Figure 7. Loss-of-chaos signature unfolding during ISO 3744 [25] testing (single engine in operation), shown together with the broadband A-weighted level (L_{Aeq}) and several TOB.

Note: The 25 Hz band (blue) shows regular modulation already at the start of the recording, suggesting a precursor of at least 15 min; some changes of condition can be seen at the 25 Hz TOB, totalizing a decrease of approximately 10 dB.

Figure 8. Loss-of-chaos signature simultaneously affecting the 25 Hz (blue) and 50 Hz (green) bands during ISO 3744 [25] testing (single engine in operation).

Note: Sudden decreases of approximately 5 dB at 25 Hz and 50 Hz are observed.

Table 1. Summary of the main characteristics of the precursor episodes documented in **Figures 5–8**.

Episode	Engine	TOB	Non-chaotic regime duration	Initial *p* (mean RMS)	Final *p* (mean RMS)	SPL change L_2–L_1
Figure 5	A	25 Hz	2,235 s (37.25 min)	0.378 Pa	0.368 Pa	−0.2 dB
Figure 6	B	25 Hz	1,589 s (26.5 min)	0.343 Pa	0.080 Pa	−13 dB
		50 Hz		0.536 Pa	0.331 Pa	−4 dB
Figure 7	A	25 Hz	1,680 s (28 min)	0.571 Pa	0.184 Pa	−10 dB
Figure 8	B	25 Hz	1,030 s (17.17 min)	0.453 Pa	0.311 Pa	−3 dB
		50 Hz		0.263 Pa	0.170 Pa	−4 dB

Table 2. Summary of the main outcomes of the exploratory analysis of the precursor episodes documented in **Figures 5–8**.

Episode	Engine	TOB	c	K_{exp}	M (300)	Standard deviation
Figure 5	A	25 Hz	1.21	1.83	104.05	0.06
Figure 6	B	25 Hz	1.18	1.29	16.973	0.13
		50 Hz	2.34	1.53	65.222	0.12
Figure 7*	A	25 Hz	1.16	1.59	330.599	0.21
			1.21	1.51	9.225	0.05
Figure 8	B	25 Hz	1.14	1.74	251.303	0.12
		50 Hz	2.28	1.61	33.167	0.07

Note: * The event in **Figure 7** was divided into two sections, according to the graphic.

The trajectories in the plane (p, q) obtained for each of the episodes and for each of the considered frequencies are presented in **Table 3**.

Table 3. Summary of the trajectories in the plane (p, q) obtained in the exploratory analysis of the precursor episodes documented in **Figures 5–8**.

Episode	Engine	25 Hz	50 Hz
Figure 5	A	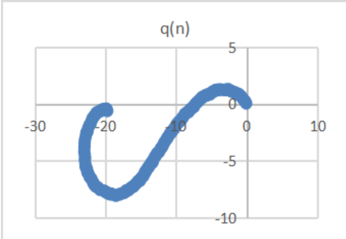	-
Figure 6	B	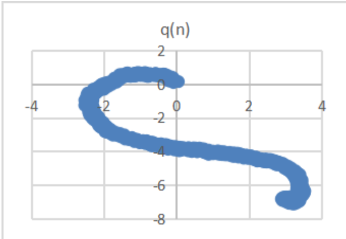	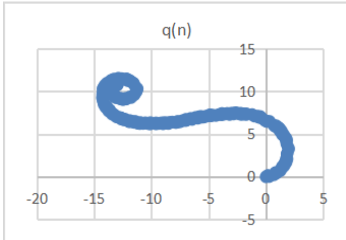
Figure 7*	A	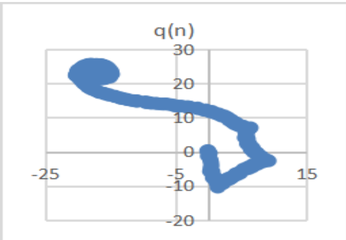 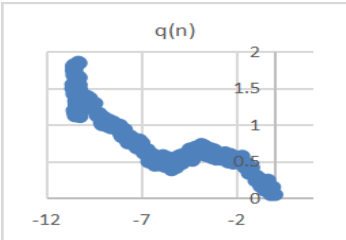	-
Figure 8	B	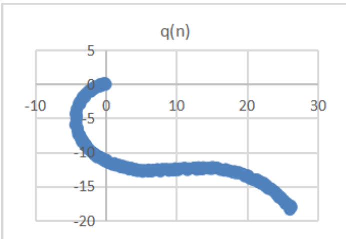	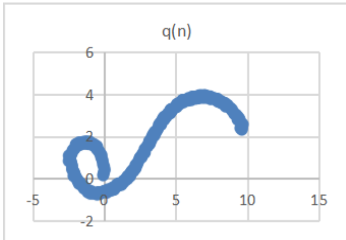

Note: * The event in **Figure 7** was divided into two sections, according to the graphic.

4. Discussion

4.1. Origin of the acoustic variability

The spectral variability documented in Section 3.1 is incompatible with a purely stationary noise source. The same engine, under identical nominal operating conditions, could produce sound pressure levels differing by up to 10 dB in individual TOB across measurements separated by only a few hours, pointing to a non-stationary, internal mechanism. The simultaneous observation of large fluctuations in the fuel inlet pressure (Section 3.2) provides a coherent physical explanation: the redesign of the combustion chambers and the introduction of the turbocharger group could have modified the conditions under which combustion takes place, creating a configuration susceptible to thermoacoustic coupling between fuel mass-flow oscillations, heat release and the chamber acoustic field [6,24].

One of the two engines fitted with heat recovery boilers is involved in the analysis performed in Section 3. The present observations also confirm that, while noise emissions at medium and high frequencies are effectively controlled by the recovery boiler acting as an in-line passive silencer, the low-frequency components are not.

4.2. Spectral coincidence with firing-rate subharmonics

A relevant feature of the observations reported in Section 3 is that the bands most clearly involved in the precursor signature (25 and 50 Hz) coincide with subharmonics and harmonics of the fundamental firing rate of the engine. With twelve cylinders firing on alternate revolutions at 500 rpm, the fundamental firing rate is $6 \times 8.33 = 50$ Hz, coincident with the grid frequency; 25 Hz corresponds to the half-order subharmonic. This pattern is consistent with the well-known sensitivity of nonlinear thermoacoustic systems to integer and half-integer multiples of forcing frequency [11, 12], and it is unlikely to be coincidental that precisely these bands are systematically involved in the observed phenomena. A complementary contribution from the lowest acoustic modes of the exhaust line cannot be ruled out: for typical exhaust-gas temperatures of 350–450 °C, the local speed of sound is approximately 480–540 m/s, and the half-wavelength at 25 Hz lies between 9.6 and 10.8 m, comparable with the dimensions of the exhaust line components. A detailed modal analysis of the complete exhaust path, beyond the scope of the present case study, would be required to quantify this contribution.

4.3. The Long-timescale precursor

An observation of practical relevance in this case study concerns the duration of the precursor stage of the instability. Laboratory studies on combustor rigs, including those that introduced the 0–1 test as a diagnostic tool for combustion noise, typically report precursor times of milliseconds to seconds [26]. In the megawatt-scale installation considered here, the loss-of-chaos signature was systematically observed to persist for several minutes before the actual jump in sound pressure level took place (**Figures 5–8** and **Tables 1–3**). Actually, the non-chaotic operating condition lasts 17–37 min in the registered events.

At the end of the non-chaotic period, a jump in the sound pressure levels graphic occurred in the analysed TOB; several of them were small, while others involved a change of 10 dB or more. Nevertheless, the jumps were expected to be increasing ones, but we recorded decreasing changes in all cases. These changes cannot be called "thermoacoustic instability," as this term refers to an increase in sound pressure levels.

It must be said that the sample size is small (n = 4 fully documented episodes, covering 4 events in 25 Hz and 2 in 50 Hz TOB), but the observed pattern in the 6 cases is compatible with the loss-of-chaos exploratory test performed by Gottwald and Melbourne [22,23].

From an applied perspective, the relevant point is that such a long precursor stage would open a practical window for the implementation of feedforward control strategies that would be infeasible at laboratory timescales. However, we recorded a set of cases where the visual loss-of-chaos of the signals at 25 Hz and 50 Hz (**Figures 5–8**), and the objective outcomes of an exploratory test based on Gottwald and Melbourne [22,23] (**Tables 2** and **3**), ratified the applicability of the loss-of-chaos method for anticipating sudden changes in sound pressure levels that were related to decreasing sound pressure levels, just the opposite expected in thermoacoustic instability occurrence.

4.4. Implications for noise control design

The acoustic emission associated with episodes of large thermoacoustic oscillations should ideally be controlled at the source, that is, by avoiding abrupt changes in the operational conditions of the engines rather than only attenuating its propagation. Conventional passive control by means of in-line silencers in the propagation path is insufficient at low frequencies, as confirmed by the present observations on engines fitted with heat recovery boilers.

A suitable integrated approach is the use of hybrid systems combining passive and active elements: passive control at the output of the system to reduce the acoustic energy at medium and high frequencies, and active noise control at the source to address the low-frequency components and, ideally, to prevent the instability from developing [8,9]. The heat recovery boiler, present in two of the engines, is a recommended passive measure but does not control low-frequency emissions [21].

In an active noise control (ANC) system, the central element is the controller, which processes information from the sensors and drives the secondary acoustic source. The design effort must concentrate on this element to obtain an effective and robust system. A key feature is the early detection of the conditions leading to instability, such as the loss-of-chaos pattern described in Section 3.3, and the ability to act before the undesired phenomenon develops. ANC systems aim to generate a secondary wave whose nodes coincide with those of the primary wave but in inverted phase, so that the superposition tends to zero. The separation between the primary and secondary sources is typically required to be no greater than 0.3 λ, with best results at 0.1 λ. Given the low frequencies involved, this geometric constraint is in principle achievable: for instance, the control of a 25 Hz wave requires a separation no greater than approximately 4 m [8,21]. This distance was available in all the engines in the studied layout; even a site-specific feasibility study would nevertheless be needed to select the best operative point to install the actuators.

A feedforward control architecture is proposed, in which the detection sensor is located on the fuel pressure line and communicates with the controller, which emits the secondary wave as soon as a loss-of-chaos pattern is detected. An adaptive control strategy is recommended to provide flexibility and robustness [9]. The several-minute delay between the loss of chaos and the onset of the change of regime documented in Section 3.3 is the key enabler of this strategy: it would provide the controller with ample time to act, in marked contrast to the response times of seconds typically reported in the literature, which are generally obtained in laboratory settings. The use of existing sensor systems for early detection is therefore considered crucial; in particular, the records of pressure fluctuations in the fuel supply system are highly informative and may be used to support the operational decision of when to act.

It should be emphasized that the proposed strategy was not validated in situ; thus, it should be read as a design recommendation supported by the analysis of long precursors.

4.5. Limitations and current status of the installation

Several limitations of the present work are explicitly acknowledged. First, the diagnostic application of the 0–1 test is exploratory (Section 2.3); the available access to raw signals was only to the 1-s series of sound pressure levels recorded in broad band and in TOB; thus, we met an approach to the value of K(t) we called K_{exp} (**Table 2**). Second, the fully documented precursor episodes (n = 4) constitute a small sample and should be interpreted as evidence of a phenomenon on which only scarce literature is available about full-scale cases. Third, no direct measurement of in-cylinder pressure or local heat-release rate was available; the inference of internal thermoacoustic coupling is supported indirectly by the fuel inlet pressure fluctuations.

The experimental measurements underlying the present study were collected more than ten years ago, in the original configuration of the installation, in the framework of a technical assistance contract that imposed strict confidentiality provisions on both the raw data and the derived findings. Publication was accordingly deferred until these provisions could be lifted, which occurred regarding major maintenance operations and changes in the configuration of the system. The interval that has elapsed between data collection and the present publication does not affect the scientific validity of the observations, which remain of interest given the persistent scarcity of full-scale acoustic measurements on megawatt-class reciprocating installations operating under thermoacoustic instability. The current status of the installation differs in important respects from that documented during the experimental campaign. At the time of writing, only seven of the original eight engines remain in operation; all of them have undergone major maintenance interventions that may have altered their acoustic behaviour with respect to the measurements reported here. Furthermore, the turbocharger units are no longer in service. The present case study should therefore be read as a documented record of the acoustic phenomena observed in the original configuration of a megawatt-class installation—a class of data that remains scarce in the open literature—and as the basis for the design considerations discussed above; it does not describe either the current layout or the operational state of the installation.

5. Conclusion

The diagnosis of the acoustic anomaly described in this case study was non-trivial. Once the acoustic instabilities developing inside the combustion chambers were identified as the underlying mechanism, the previously disconnected observations—spectral variability between measurements, discrepancies with respect to acoustic modelling, and fluctuations of the fuel inlet pressure—became internally consistent, and a clear noise-control strategy could be formulated.

Each quasi-stationary regime preceding and following an episode of change of the thermoacoustic operational condition extends over several minutes, as does the transition between the two regimes. The bands most strongly affected by both the steady-state variability and the precursor signature coincide with subharmonics and harmonics of the engine firing rate (50 Hz), which provides a plausible mechanistic interpretation of why these particular bands are systematically involved.

The numerical application of the 0–1 test to objectively explore the episodes of loss-of-chaos allowed us to ratify an outcome different from what was foreseeable: given all the features for anticipating a thermoacoustic instability, a sudden decrease in sound pressure levels was registered in every case. This opens the applicability of the tool for anticipating other abrupt changes of regime, all of them being undesirable for the operation of the engines.

Active noise control is identified as a particularly suitable strategy to address the low-frequency emissions associated with the instability. A hybrid noise-control system is proposed as a design recommendation, combining a passive stage at the output of the engines to control medium and high frequencies with an active feedforward stage at the source to address the low-frequency components and, ideally, to prevent the instability from developing. The time available for the controller to act, of the order of several minutes rather than seconds, is the operational feature that makes the proposed strategy potentially feasible in the megawatt-scale regime considered here.

Author contributions: Conceptualization, AEG, PGK and HCV; methodology, AEG; field data, PGK; formal analysis, AEG and PGK; investigation, AEG, PGK and HCV; data curation, AEG and PGK; writing—original draft preparation, AEG, PGK and HCV; writing—review and editing, AEG, PGK and HCV; supervision, AEG; project administration, AEG; funding acquisition, AEG. All authors have read and agreed to the published version of the manuscript.

Funding: This research was funded by a technical assistance contract between Fundación Julio Ricaldoni and the National Energy Agency.

Institutional review board statement: Not applicable.

Informed consent statement: Not applicable.

Data availability statement: The data underlying this study are not publicly available due to contractual restrictions associated with the technical assistance contract under which the measurements were performed.

Conflicts of interest: The authors declare no conflicts of interest.

AI use statement: During the preparation of this manuscript, the authors used AI tools solely for language refinement. No AI tools were used for data analysis, interpretation, or generation of scientific content. All outputs were critically reviewed and edited by the authors. The authors take full responsibility for the integrity and accuracy of the work.

Abbreviation

ANC	Active Noise Control
L_{Aeq}	A-weighted equivalent continuous sound pressure level
LES	Large Eddy Simulation
L_{Zeq}	Z-weighted equivalent continuous sound pressure level
SPL	Sound Pressure Level
TOB	One-Third Octave Band

References

1. Sawilam M, Babaa S, Haddabi A, et al. Noise Control Solutions for Diesel Generator Sets. Journal of Power and Energy Engineering. 2023; 11: 36–43. doi: 10.4236/jpee.2023.1112003
2. Gentil YY, Daviller G, Moreau S. Combustion noise modelling re-examined for thermally perfect and multi-species gas flows. In: Proceedings of the 30th AIAA/CEAS Aeroacoustics Conference (2024); 4–7 June 2024; Rome, Italy. doi: 10.2514/6.2024-3328
3. Mitigating Combustion-driven Oscillation (Thermoacoustic Instability) in Industrial Combustors. Available online: https://deicon.com/mitigating-combustion-driven-oscillation-thermoacoustic-instability-in-industrial-combustors/ (accessed on 25 May 2026).
4. Strahle WC. Combustion noise. Progress in Energy and Combustion Science. 1978; 4(3): 157–176. doi: 10.1016/0360-1285(78)90002-3
5. Litak G, Taccani R, Radu R, et al. Estimation of a noise level using coarse-grained entropy of experimental time series of internal pressure in a combustion engine. Chaos, Solitons and Fractals. 2005; 23(5): 1695–1701. doi: 10.1016/S0960-0779(04)00434-5
6. Schuermans B, Moeck J, Blondé A. The Rayleigh integral is always positive in steadily operated combustors. Proceedings of the Combustion Institute. 2023; 39(4): 4661–4669. doi: 10.1016/j.proci.2022.08.035
7. Livebardon T, Moreau S, Poinsot T, et al. Numerical investigation of combustion noise generation in a full annular combustion chamber. In: Proceedings of the 21st AIAA/CEAS Aeroacoustics Conference; 22–26 June 2015; Dallas, TX, USA. doi: 10.2514/6.2015-2971
8. Dowling AP, Morgans AS. Feedback control of combustion oscillations. Annual Review of Fluid Mechanics. 2005; 37: 151–182. doi: 10.1146/annurev.fluid.36.050802.122038
9. McManus KR, Poinsot T, Candel SM. A review of active control of combustion instabilities. Progress in Energy and Combustion Science. 1993; 19(1): 1–29. doi: 10.1016/0360-1285(93)90020-F
10. Poinsot T. Prediction and control of combustion instabilities in real engines. Proceedings of the Combustion Institute. 2017; 36(1): 1–28. doi: 10.1016/j.proci.2016.05.007
11. Juniper MP, Sujith RI. Sensitivity and nonlinearity of thermoacoustic oscillations. Annual Review of Fluid Mechanics. 2018; 50: 661–689. doi: 10.1146/annurev-fluid-122316-045125
12. Sujith RI, Unni VR. Complex system approach to investigate and mitigate thermoacoustic instability in turbulent combustors. Physics of Fluids. 2020; 32(6): 061401. doi: 10.1063/5.0003702
13. Broatch A, Novella R, García-Tíscar J, et al. Analysis of combustion acoustic phenomena in compression-ignition engines using large eddy simulation. Physics of Fluids. 2020; 32(8): 085101. doi: 10.1063/5.0011929
14. Magri L. Adjoint methods as design tools in thermoacoustics. Applied Mechanics Reviews. 2019; 71(2): 020801. doi: 10.1115/1.4042821
15. Deshmukh NN, Ansari A, Tajir AP, et al. Suppression of thermo-acoustic instabilities in horizontal Rijke tube using pulsating radial jets. MethodsX. 2023; 11: 102325. doi: 10.1016/j.mex.2023.102325
16. Deshmukh NN, Ansari A, Kumar P, et al. Development of closed-loop active control method for suppression of thermoacoustic instability using radial air micro-jets. MethodsX. 2023; 10: 102123. doi: 10.1016/j.mex.2023.102123
17. Zhu Z, Zhu J, Fang Y, et al. Passive control of thermoacoustic instability in a high-efficiency domestic gas stove with fine-tuning burner. Case Studies in Thermal Engineering. 2024; 62: 105209. doi: 10.1016/j.csite.2024.105209
18. George NB, Raghunathan M, Unni VR, et al. Preventing a global transition to thermoacoustic instability by targeting local dynamics. Scientific Reports. 2022; 12: 9305. doi: 10.1038/s41598-022-12951-6
19. Deng J, Li T, Wang J, et al. Experimental Study of Suppressing the Thermoacoustic Instabilities in a Rijke Tube Using Microsecond Discharge Plasma. Aerospace. 2022; 9(12): 836. doi: 10.3390/aerospace9120836
20. Gosavi A, Priyam A. Vibration and Noise Reduction in Internal Combustion Engines Using Active Control Techniques: A Survey. RERIC Proceedings. 2025; (1): 89–94. doi: 10.64289/rericproc.25.0105.7853288
21. González AE, Cataldo Ottieri J, Gianoli Kovar P, et al. Measuring sound pressure levels during thermoacoustic instabilities in large engines: Case study. Journal of Modern Physics. 2017; 8(10): 1685–1699. doi: 10.4236/jmp.2017.810099
22. Gottwald GA, Melbourne I. A new test for chaos in deterministic systems. Proceedings of the Royal Society A: Mathematical, Physical and Engineering Sciences. 2004; 460(2042): 603–611. doi: 10.1098/rspa.2003.1183

23. Gottwald GA, Melbourne I. On the implementation of the 0–1 test for chaos. SIAM Journal on Applied Dynamical Systems. 2009; 8(1): 129–145. doi: 10.1137/080718851
24. Schuermans B. Modeling and Control of Thermoacoustic Instabilities [PhD thesis]. École Polytechnique Fédérale de Lausanne; 2003.
25. ISO 3744:2010. Acoustics—Determination of sound power levels and sound energy levels of noise sources using sound pressure—Engineering methods for an essentially free field over a reflecting plane. International Organization for Standardization; 2010.
26. Nair V, Thampi G, Karuppusamy S, et al. Loss of chaos in combustion noise as a precursor of impending combustion instability. International Journal of Spray and Combustion Dynamics. 2013; 5(4): 273–290. doi: 10.1260/1756-8277.5.4.273
27. Moysis L. 0–1 Test for Chaos for Discrete Maps. MATLAB Central File Exchange; 2026. Available online: https://la.mathworks.com/matlabcentral/fileexchange/157591-0-1-test-for-chaos-for-discrete-maps